ACS OMEGA

http://pubs.acs.org/journal/acsodf

Article

Optical Anisotropy and Momentum-Dependent Excitons in Dibenzopentacene Single Crystals

Lukas Graf,* Fupin Liu, Marco Naumann, Friedrich Roth, Bipasha Debnath, Bernd Büchner, Yulia Krupskaya, Alexey A. Popov, and Martin Knupfer

Cite This: *ACS Omega* 2022, 7, 21183−21191

Read Online

ACCESS | Metrics & More | Article Recommendations | Supporting Information

ABSTRACT: High-quality single crystals of the organic semiconductor (1,2;8,9)-dibenzopentacene were grown via physical vapor transport. The crystal structure—unknown before—was determined by single-crystal X-ray diffraction; polarization-dependent optical absorption measurements display a large anisotropy in the *ac* plane of the crystals. The overall Davydov splitting is ∼110 meV, which is slightly lower than that in the close relative pentacene (120 meV). Momentum-dependent electron energy-loss spectroscopy measurements show a clear exciton dispersion of the Davydov components. An analysis of the dispersion using a simple 1D model indicates smaller electron- and hole-transfer integrals in dibenzopentacene as compared to pentacene. The spectral weight distribution of the excitation spectra is strongly momentum-dependent and demonstrates a strong momentum-dependent admixture of Frenkel excitons, charge-transfer excitons, and vibrational modes.

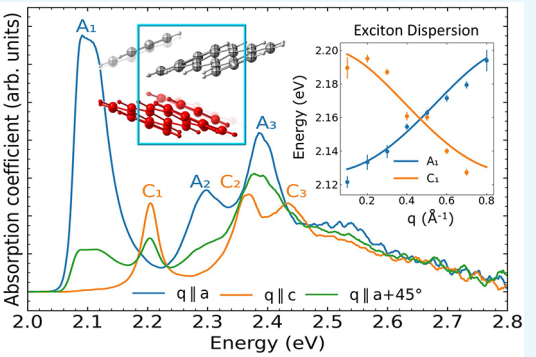

1. INTRODUCTION

The family of Oligoacenes includes many promising organic semiconductors, such as anthracene, tetracene, and pentacene. All show relatively high charge-carrier mobilities[1−4] and are already used for applications such as organic light-emitting diodes, organic field-effect transistors, and organic solar cells.[5−8] Moreover, they represent model compounds for the whole class of organic semiconductors, and their investigation led to important insights into the physics of these materials.[9−18]

The optoelectronic properties of organic semiconductors are mostly driven by excitons, bound electron−hole pairs, lowered in energy by the Coulomb attraction and sitting on one single molecule (Frenkel exciton) or on two adjacent molecules (charge-transfer (CT) exciton). Exciton dynamics is a subject of high interest, and it has been shown in recent works that in oligoacenes neither the exciton dispersion nor the Davydov splitting (DS), an energy level splitting due to symmetrically inequivalent molecules in the unit cell,[19] can be explained by the molecular Frenkel exciton picture only[17,20−36] but instead are explained with an intermixing of Frenkel, CT excitations, and vibrational modes. The latest theoretical descriptions on pentacene and tetracene by the group of Spano and co-workers[17,34−36] implemented this idea of an intermixing successfully into a model that describes the experimental data on tetracene and pentacene very well. On the basis of a detailed understanding of the exciton behavior in single crystals, it is also possible to predict exciton migration as it must occur, e.g., in organic solar cells for a high performance.

Starting from the well-known pentacene system, we choose 1,2;8,9-dibenzopentacene, a pentacene derivate with 2 more benzene rings, placed on the diagonal ends on the long axis of the pentacene molecule. It has strong similarities in the electron π-system with pentacene.[37−39] Not as present as other Oligoacenes in research, dibenzopentacene (DBP) only received some attention as a potential superconductor[40−42] in the past. On the other hand, dibenzopentacene offers the possibility to investigate the anisotropic exciton dispersion in a molecular crystal made out of molecules with a lower symmetry than that of pentacene.

To the best of our knowledge, the growth and characterization of 1,2;8,9-dibenzopentacene single crystals were not reported yet. Polarized optical absorption measurements show a strong anisotropy, and momentum-dependent electron energy-loss spectroscopy (EELS) measurements reveal the exciton dispersion in two lattice directions. Our results demonstrate that the exciton physics in dibenzopentacene is determined by a strong coupling of Frenkel and CT excitons.

Received: March 31, 2022
Accepted: May 24, 2022
Published: June 8, 2022

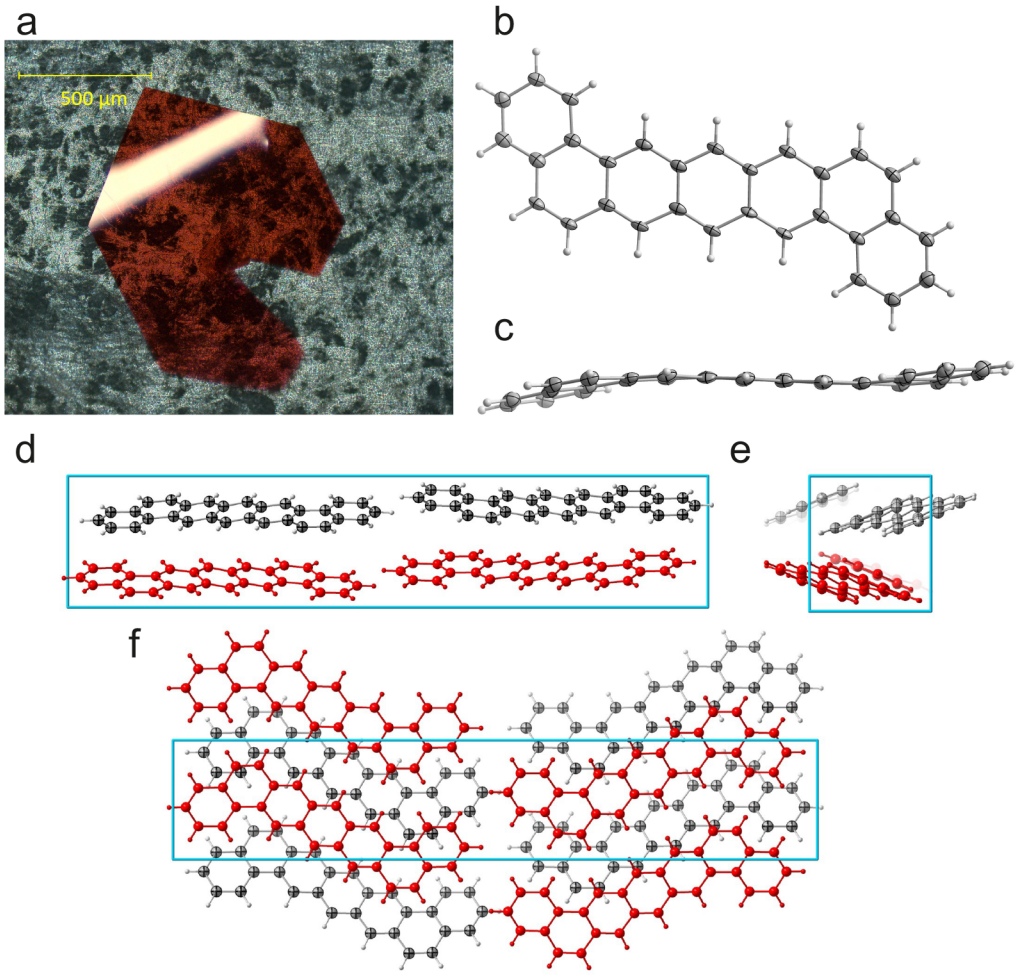

Figure 1. (a) Optical picture of the grown dibenzopentacene crystal. (b) Dibenzopentacene molecule drawing at 30% ellipsoid probability. Color code: gray for carbon and white for hydrogen. (c) Dibenzopentacene molecule from the side to show the dihedral angle (nonplanar molecular structure). (d) Molecular packing of the single crystal in the *ab* plane. (e) Molecular packing in the *ac* plane. (f) Molecular packing in the *bc* plane. To guide the vision, one layer of the molecules is highlighted with red and the unit cell borders are lined in blue.

2. CRYSTAL GROWTH AND EXPERIMENTAL DETAILS

Dibenzopentacene single crystals were grown using physical vapor transport (PVT) in a furnace surrounded by a resistive heater to set up a temperature gradient at atmospheric pressure.[43] Pure argon gas, 15 sccm, was used as the purging gas. Dibenzopentacene molecules (purchased from TCI Germany) were heated in the hot zone at 303 °C for 2−7 days, depending on the desired size and thickness of the crystal. Single crystals then could be collected in the crystallization zone of the furnace and processed further for measurements. The crystals showed very homogeneous shape/color, so polymorphism could be excluded.

X-ray diffraction data collection was carried out at the BESSY II storage ring (BL14.2, Berlin-Adlershof, Germany).[44] XDSAPP2.0 suite was employed for data processing.[45,46] The structure was solved by direct methods and refined by SHELXL-2018.[47] Hydrogen atoms were added geometrically and refined with a riding model.

For optical absorption measurements, we transferred the crystals onto a glass substrate and measured the absorption spectra using a Bruker vertex spectrometer in the UV−vis and IR range at 77 K. Electron diffraction and EELS were performed with a custom-made electron energy-loss spectrometer, which could detect electronic excitations as a function of momentum transfer.[48,49] The primary electron energy was 172 keV. To keep organic single crystals undamaged as long as possible, the sample temperature was always kept at 20 K, which also minimized thermal broadening in the spectra. Every sample was checked regularly for sample degradation to avoid distorted data. Electron diffraction was applied in situ prior to every measurement to ensure the quality of the sample and conformance with the measured crystal structure (see Figure 4a).

With an energy and momentum resolution of about 85 meV and 0.035 $Å^{-1}$, the measured signal in EELS is proportional to the loss function $\mathrm{Im}(-1/\epsilon(q, \omega))$ and can be determined for different momentum transfers q. With increasing the momentum transfer q, the EELS cross section decreases proportionally to $\sim\frac{1}{q^2}$.

3. RESULTS AND DISCUSSION

3.1. Crystal Structure. The color of the crystal is light pink, compared to the dark burgundy-red of the source material (see Figure 1a). DBP grows in flakelike crystals in the crystal *ac* plane. In crystals of our desired thickness (50−200 nm for EELS measurements), they tend to roll up or stick to

https://doi.org/10.1021/acsomega.2c01987
ACS Omega 2022, 7, 21183−21191

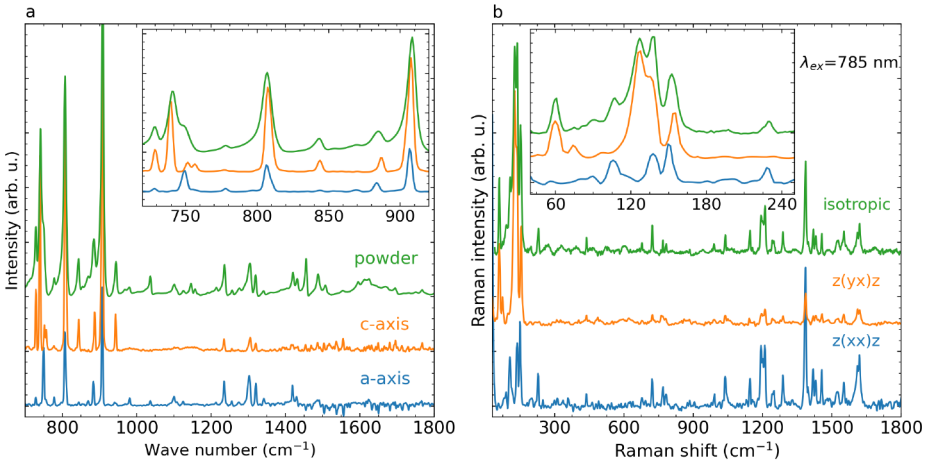

Figure 2. (a) IR spectra of the dibenzopentacene crystal with a polarization of the incoming light according to the crystal's *a* and *c* axes and with a powder spectra in comparison. The inset shows a zoomed-in region to display the strong polarization dependence. (b) Raman spectra with two polarization directions of the incoming beam, an averaged isotropic curve, and an inset with an example region to demonstrate the differences of the spectra.

each other. The process of rolling up seems uncontrollable. X-ray diffraction (XRD) measurements revealed the crystal structure for the first time. The crystal system is orthorhombic with the space group $P2_12_12$ and the crystal axis having the length a = 7.48 Å, b = 36.38 Å, and c = 6.72 Å. The unit cell contains 4 molecules; two molecules are pi-stacked with an small angle (see Figure 1d and e) in the *ac* plane, similar to the typical herringbone packing of pentacene.[50] Both of these pairs connect to each other on the long molecular axis under an angle (see Figure 1d and f) in the *b* direction. The two phenyl rings at both ends of the molecule have a dihedral angle of ∼4°. According to previous data on nonplanarity, this behavior is not rare in the family of oligoacenes[50] (see Figure 1c). The complete crystal structure data are given in the Supporting Information.

For further crystal characterization, we performed IR and Raman spectroscopy on the dibenzopentacene crystal. The IR data are presented in Figure 2a and consist of the IR spectra in the two lattice directions *a* and *c* and a nonpolarized powder spectra. The Raman data are given in Figure 2b and show two curves with different polarizations of the incoming beam ($z(yx)z$ and $z(xx)z$) and a third curve that is averaged over all angles and therefore nonpolarized (isotropic). Both data sets are strongly polarization-dependent, as can be seen in detail in the figure's inset. This strong polarization dependence demonstrates that our crystals are of high quality.

3.2. Electronic Excitations in the Optical Limit. Dibenzopentacene molecules were dissolved and diluted in toluene until the absorption spectra showed no sign of intermolecular excitations. Figure 3a shows the measured spectra. The (0−0) excitation at 2.34 eV is followed by a vibronic progression. The data indicate that this progression is composed of two vibrational modes, as is visible at the (0−1) and (0−2) peaks. The main mode has a vibrational energy of ∼178 meV, while the second mode, visible in (0−1) as a shoulder, has a slightly reduced energy of ∼145 meV. This is in accordance with earlier measurements on solution-phase dibenzopentacene.[51] The appearance of vibrational satellites is a well-known feature in the excitation spectra of organic semiconductor molecules; see, for instance, the corresponding data for pentacene and tetracene in solution.[27,35]

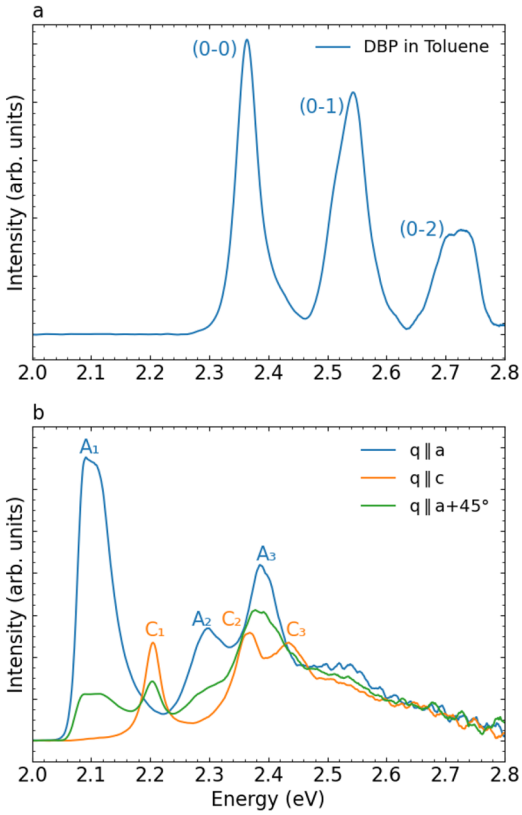

Figure 3. Optical absorption spectra of dibenzopentacene molecules in toluene solution (a) in comparison to the polarization-dependent optical absorption spectra of a dibenzopentacene single crystal (b). The crystal data reveal a strong anisotropy of the absorption as a function of light polarization.

Upon crystallization the spectra change strongly, as shown in Figure 3b. Three curves are shown, measured with linearly polarized light at 77 K. The blue curve shows the spectra with a light polarization in the direction of the crystal *a* axis, the orange curve is in the direction of the *c* axis, and the green curve was measured at 45° between these axes to clarify the change between the two spectra. The crystal structure has 4

https://doi.org/10.1021/acsomega.2c01987
ACS Omega 2022, 7, 21183−21191

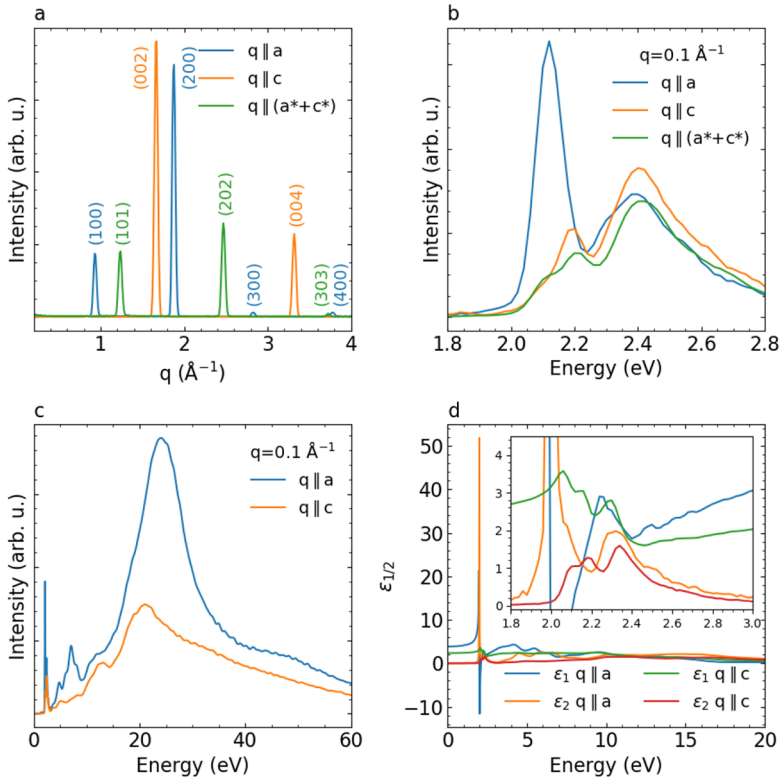

Figure 4. (a) Electron diffraction profiles of dibenzopentacene along three reciprocal lattice directions, which are parallel to the *a*, *c*, and (*a** + *c**) directions, due to the orthorhombic crystal symmetry. These data demonstrate that the crystal is of high quality. (b) Electronic excitation spectra (loss function) of dibenzopentacene as measured using EELS in the optical limit (q = 0.1 Å^{-1}) for three momentum vector directions. (c) Wide energy EELS data in the optical limit for momentum directions parallel to the crystal *a* and *c* axes. (d) Real part, ϵ_1, and imaginary part, ϵ_2, of the dielectric function of dibenzopentacene for momentum vectors parallel to the crystal *a* and *c* axes as obtained via a Kramers−Kronig analysis. The inset shows a zoomed-in region to denote more features.

molecules in the unit cell, which are arranged in two very similar herringbone-like planes, tilted slightly to each other in the *b* direction. We therefore note that measurements in the *ac* plane always represent both planes in the unit cell. Due to the $P2_12_12$ space group, which corresponds to D_2 point symmetry, we would expect two Davydov components in the *ac* plane polarized along the two axes.

The peaks in the absorption data for light polarization parallel to the *a* and *c* directions are labeled with A_1, A_2, and A_3 and C_1, C_2, and C_3. At first sight, the polarization-dependent absorption data are strongly anisotropic and undergo a strong red-shift compared to the solution-phase data due to solid-state polarization effects.[52] The feature A_1 has a peak energy of 2.09 eV. We ascribe the broad appearance of feature A_1 to the fact that the transmittivity of a parallel-sided plane (our crystal) is determined by the interplay of transmission and multiple reflections.[53−55] Peak A_2 at 2.3 eV is the first peak of the vibronic progression. The following peak A_3 at 2.39 eV, however, cannot be associated with a vibronic satellite because its energy position does not agree. We instead conclude that it is of electronic origin.

Turning the light polarization by 90°, the spectrum changes dramatically. Peak A_1 vanishes completely, and instead peak C_1 at 2.2 eV arises. This peak is the second Davydov component and therefore defines the Davydov splitting (DS) as 110 meV, which is a bit lower than that in the close relative pentacene of 120 meV at a similar sample temperature.[35,56] Similar to A_3, peaks C_2 and C_3 cannot be associated with simple vibronic satellites.

Compared to single-crystal data from tetracene[57] and pentacene,[35,56] tetracene shows a regular vibronic progression, while the pentacene spectra show an irregular satellite region when compared to the solution data. For pentacene, it has been shown that the entire excitation region can be well-described by a substantial coupling of molecular Frenkel and CT excitons within a multiparticle basis set in addition to the vibronic coupling.[34,35] For dibenzopentacene we expect a similar behavior, particularly regarding the satellite region above 2.3 eV in both directions. This will be further discussed later. The electronic excitation spectra of dibenzopentacene crystals have also been probed using EELS for momentum vectors in the *ac* plane of the crystal. The corresponding data have been taken at 20 K. The momentum vector has been aligned to the respective crystal directions with the help of the electron diffraction profiles measured in situ in our spectrometer. Figure 4a depicts the electron diffraction profiles along selected reciprocal directions. The data reveal the corresponding Bragg diffraction features and document the single-crystalline nature of our samples.

In Figure 4b we present the electronic excitation spectra at a small momentum value of 0.1 Å^{-1}, which represents the optical limit, as well as spectra for momentum vectors aligned parallel to the *a* and *c* crystal directions and the (*a** + *c**) reciprocal crystal direction. The data are in good agreement with those from optical absorption (see earlier) but do not show the fine structure due to a lower energy resolution. The data can also be compared to thin-film data,[37] which show a similar energy onset but not the angle dependence of the single crystals. In

https://doi.org/10.1021/acsomega.2c01987
ACS Omega 2022, 7, 21183−21191

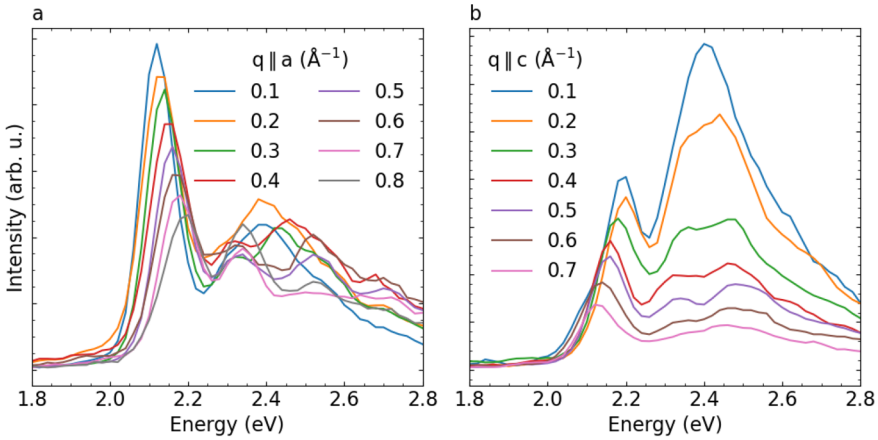

Figure 5. Electronic excitation spectra of dibenzopentacene crystals measured using EELS as a function of increasing momentum parallel to the crystal *a* (a) and *c* axes (b). Data curves are smoothed to obtain better clarity (see the Supporting Information).

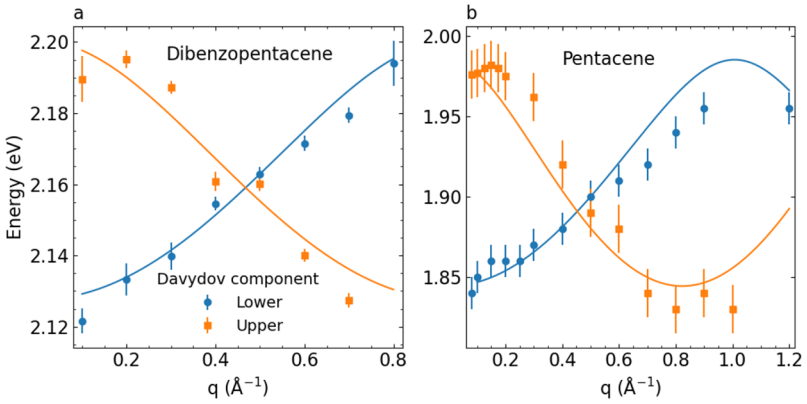

Figure 6. Dispersion of the lowest singlet excitons in dibenzopentacene and pentacene (data taken from paper by Roth et al.[63]) for momentum transfers parallel to the *a* and *c* axes of the dibenzopentacene crystal and the *a* and *b* axes of pentacene, respectively. The solid lines represent the results of the dispersion analysis using a one-dimensional model proposed by Hestand et al.[35] (see text).

detail, the data for a momentum vector parallel to the *a* axis are characterized by an onset at ∼2 eV and a strong excitation at 2.1 eV (A_1). Excitation A_2 is seen as a shoulder at 2.3 eV only, while excitation A_3 still is represented by a clear maximum at 2.4 eV. For momentum vectors parallel to the crystal *c* axis, the first spectral structure C_1 appears at 2.2 eV followed by a broader feature at 2.4 eV being composed of features C_2 and C_3 as seen in the optical absorption.

As our EELS spectrometer allows measurements in a large energy range, it is possible to determine the loss function ($\mathrm{Im}(-1/\epsilon(q,\omega))$) related to all valence excitations. In Figure 4c we show such data for a small momentum-transfer value along the two crystal directions *a* and *c*. The two curves are dominated by a broad maximum between 20 and 24 eV, which can be ascribed to the so-called valence band plasmon. This plasmon is due to a collective excitation of all valence electrons. The energy position at which it is observed is typical for π-conjugated solids.[58−60] The real and imaginary parts of the dielectric function, ϵ_1 and ϵ_2, can be derived via a Kramers−Kronig analysis of the loss function after subtraction of the elastic line.[48] We have used the oscillator sum rule to normalize the Kramers−Kronig analysis. In Figure 4d we present the results for ϵ_1 and ϵ_2 in a wide energy range with an inset that shows the energy window of the lowest excitations. The obtained values for $\epsilon_1(0)$ reveal the anisotropic refractive index ($n = \sqrt{\epsilon_1(0)}$) for dibenzopentacene in the *ac* plane: n_a = 1.96 and n_c = 1.52.

3.3. Exciton Dispersion. The evolutions of the excitation spectra for increasing momentum parallel to the *a* and *c* axes are depicted in parts a and b of Figure 5, respectively. These data clearly demonstrate a significant momentum dependence of the spectra. We first concentrate on the energy position of the lowest excitation (A_1 and C_1), which provides the exciton dispersion or exciton band structure of the lowest singlet exciton in dibenzopentacene. For momentum vectors parallel to the *a* axis, we observe a clear up-shift of the exciton energy. The spectral width of the exciton feature remains rather constant. For momentum vectors parallel to the *c* axis, a significant down-shift (negative) dispersion is seen, and the exciton feature below 2.2 eV again is a well-defined, symmetric spectral feature, independent of the momentum value.

The data in parts a and b of Figure 5 are very similar to what has been observed for the exciton dispersion in tetracene[61,62] and especially in pentacene single crystals.[29,63] This is not surprising in view of the similarities in the molecular-packing habits in the crystals. In Figure 6a, we show a summary of the exciton dispersion in dibenzopentacene, whereas the peak positions in parts a and b of Figure 5 have been determined by fitting the peak with a Gaussian function. To underline the close similarity of the exciton dispersion to pentacene, we have

https://doi.org/10.1021/acsomega.2c01987
ACS Omega 2022, 7, 21183−21191

taken the peak centers of the two Davydov components of pentacene (data taken from paper by Roth et al.[63]) and show it in a side-by-side comparison in Figure 6b.

The exciton behavior and wave function in pentacene were analyzed in detail by Spano and co-workers,[35] and they have provided detailed insight into the origin and the nature of the respective spectral features. Furthermore, they have provided a simplified one-dimensional model for the exciton dispersion, which covers the essential information on the exciton band structure arising from the mixing between Frenkel and charge-transfer excitons while the Coulomb coupling is negligible. Within this effective exciton model, the dispersion is governed by the electron and hole hopping integrals to the nearest neighbor, t_e and t_h:[35]

$$E_{+/-}(k) = \omega_{0-0} + \Delta_{+/-}(k) \tag{1}$$

$$\Delta_{+}(k) = \frac{E_{CT}}{2} - \sqrt{2({t_e}^2 + {t_h}^2) + 4t_e t_h \cos(k/2) + {E_{CT}}^2/4} \tag{2}$$

$$\Delta_{-}(k) = \frac{E_{CT}}{2} - \sqrt{2({t_e}^2 + {t_h}^2) - 4t_e t_h \cos(k/2) + {E_{CT}}^2/4} \tag{3}$$

In this model, ω_{0-0} represents the energy for the first molecular Frenkel exciton, and the parameter E_{CT} stands for the energy difference of the charge transfer and the molecular Frenkel excitation. Importantly, the relative sign of t_e and t_h determines the band curvature in the exciton dispersion.

We have applied this simplified model in order to obtain a more quantitative insight into the exciton dispersion and thus also t_e and t_h in dibenzopentacene, in comparison to those in pentacene. To do so, we have taken into account the different lattice constants (r = a, b, or c) and replaced the argument in the cosine function in eqs 2 and 3 with $\frac{qr}{2}$. Furthermore, the energy of the charge-transfer excitation E_{CT} in pentacene can be estimated to be ∼0.2 eV, as indicated by electro-absorption measurements[22] and detailed theoretical analysis of the pentacene absorption spectra.[35] For dibenzopentacene, we assume the same value because the crystal-packing habit is very similar to that for pentacene. The molecular excitation energy ω_{0-0} can be estimated by taking the energy of the optical absorption in solution and an additional energy shift to lower energies due to crystal formation (i.e., polarization screening of the lowest excitation[35,52]). We took these into account by setting an upper limit for ω_{0-0} of 2.24 eV for dibenzopentacene and 2.01 eV for pentacene.

With these values, our data on the exciton dispersion in dibenzopentacene and pentacene can be successfully fitted with these equations. The fit was done with $t_e = t_h$ and $t_e \neq t_h$; the results were virtually independent, and we only show those for $t_e = t_h$ in Table 1, as both fits resulted in the same values.

Table 1. Results of the Fit of the Exciton Dispersion, As Described in the Text (See Also Figure 6)

	ω_{0-0} (eV)	t_e (eV)	t_h (eV)
dibenzopentacene	2.20	0.050	0.050
pentacene	1.99	0.077	0.077

The results of our fit confirm what is seen in Figure 6. ω_{0-0} is larger for dibenzopentacene, in agreement with the larger absorption energy of the solution data. In both materials, t_e and t_h have the same sign and are of virtually the same value. In other words, the exciton behaviors in the two compounds are also very similar. The absolute values of t_e and t_h are ∼36% smaller in dibenzopentacene compared to pentacene, which results in a smaller exciton bandwidth. Further, this also indicates that electron and hole mobilities may be somewhat smaller in dibenzopentacene.

3.4. Spectral Weight Analysis. As mentioned earlier, parts a and b of Figure 5 demonstrate significant momentum-dependent variation of the spectral shape or the intensity distribution among the various spectral features. We emphasize that the spectral shape is somehow irregular as compared to the well-known appearance of vibronic satellites in the absorption spectra of individual organic semiconductor molecules (e.g., in solution, as shown for dibenzopentacene earlier). Thus, the excitation spectra of dibenzopentacene (and also of pentacene) cannot be rationalized upon coupling to molecular vibrations only. Indeed, the detailed theoretical analysis of the pentacene spectra by Spano and co-workers[34,35] has shown that the complete excitation region can be well-understood by a substantial coupling of molecular Frenkel and CT excitons within a multiparticle basis set in addition to the vibronic coupling, and this coupling also determines the exciton dispersion (see earlier). We analyzed the spectral weight distribution of the lowest excitations as a function of momentum parallel to the lattice directions a and c in dibenzopentacene. The same analysis was carried out for the data that were obtained for pentacene earlier.[63] (Note that the respective lattice directions in pentacene are denoted as a and b axes.) For our analysis, the measured EELS data were multiplied by the excitation energy to obtain data sets that are proportional to $[\omega \times \mathrm{Im}(-1/\epsilon(\omega))]$ because this function represents the oscillator sum rule.[64] Further, we determined the total spectra weight (I_{total}) by integrating these data in an energy window from 1.96 to 3 eV for dibenzopentacene and from 1.64 to 2.9 eV for pentacene. Finally, the spectral weight of the lowest, well-defined exciton ($I_{exciton}$) has been derived by fitting a Gaussian function to this lowest-energy region. This allows the determination of the intensity ratio of the lowest exciton feature and the following satellite region:

$$\frac{I_{exciton}}{I_{satellite}} = \frac{I_{exciton}}{I_{total} - I_{exciton}} \tag{4}$$

Figure 7 shows the results of this analysis. It reveals that the spectral weight distribution between the lowest exciton and the satellite region is significantly momentum- and direction-dependent. For both dibenzopentacene and pentacene and for small momentum transfer, $I_{exciton}$ represents a quite large portion of the total spectral weight for momenta along the a direction, but it is much smaller for a momentum parallel to the c axis in dibenzopentacene and the b axis in pentacene. This is in very good agreement with the optical measurements of dibenzopentacene and pentacene[35,56] as a function of polarization. According to Hestand et al.[35] the spectral weight distribution is a direct consequence of the exciton coupling and the admixture of Frenkel and CT excitons and the vibrations. In the optical limit, the dominating exciton coupling is provided by CT coupling, i.e., by electron- and hole-transfer processes, and the resulting exciton spectral weight distribution

https://doi.org/10.1021/acsomega.2c01987
ACS Omega 2022, 7, 21183−21191

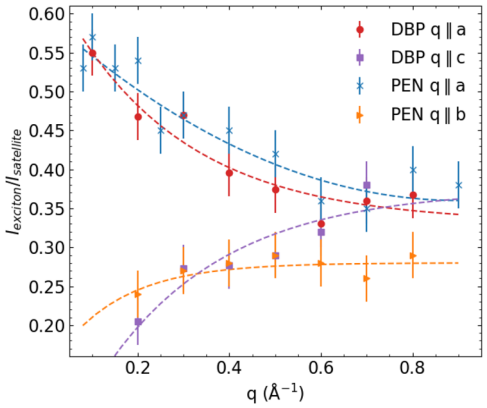

Figure 7. Relative spectral weight of the lowest exciton feature and the following satellite region in the excitation spectra of dibenzopentacene and pentacene as a function of momentum transfer and direction. The dashed lines are included as a guide to the eye.

sensitively depends on the relative signs of the electron- and hole-transfer integrals (t_e and t_h), which connect the differently oriented molecules in the unit cell.[35]

Electron- and hole-transfer integrals, t_e and t_h, in dibenzopentacene and pentacene have the same sign (see paper by Hestand et al.[35] and our dispersion analysis earlier); therefore, the coupling near $q = 0$ is large and results in a charge-transfer J-aggregate-like behavior of the excitons for q (or polarization) parallel to the a axis. It has also been pointed out that the coupling of Frenkel and CT excitons is momentum-dependent. Coupling of Frenkel and CT excitons is provided by a charge separation, and the corresponding matrix element is proportional to $|t_e + t_h \exp(i\tilde{q})|$ ($\tilde{q}$ is the momentum relative to the reciprocal lattice constants).[36] Thus, provided that t_e and t_h are of similar absolute value, the Frenkel−CT coupling almost cancels for large q vectors parallel to a. As a consequence, the spectral redistribution at large q approaches that of the vibronic progression seen for individual molecules (see earlier). For momenta along the c direction (for pentacene, b), the Frenkel−CT coupling is very small at low q, i.e., the opposite trend is observed for the spectral weight distribution. For pentacene this has been calculated in detail previously.[35] These results clearly support the microscopic theoretical description of the excitation spectrum in pentacene by Spano and co-workers,[35] and they demonstrate the close similarity of the exciton behaviors in pentacene and dibenzopentacene.

4. CONCLUSION

We have grown high-quality single crystals of the organic semiconductor (1,2;8,9)-dibenzopentacene using physical vapor deposition. The crystals were then characterized with XRD; they crystallized in an orthorhombic crystal system with 4 molecules in the unit cell. Furthermore, these crystals grew in thin flakes in the crystal *ac* plane. IR and Raman measurements showed a strong polarization-dependence. The optical absorption was determined as a function of light polarization in the *ac* plane of the crystals. These measurements revealed a strong anisotropy and a Davydov splitting of ∼110 meV. Momentum-dependent EELS measurements were performed for momentum vectors parallel to the a and c axes. The first excitations were characterized by a clear exciton dispersion, similar to what has been reported and theoretically analyzed for pentacene and tetracene.[29,34,35,61−63] The dispersion was analyzed using a one-dimensional model proposed by Hestand et al.[35] In comparison to pentacene, this analysis revealed that electron- and hole-transfer integrals in dibenzopentacene were smaller (by ∼36%) than in the close relative pentacene, which indicated a smaller charge carrier mobility. Finally, a spectral weight analysis of the EELS data of dibenzopentacene and pentacene demonstrated a significant momentum dependence of the irregular satellite region, which was due to strong coupling of molecular Frenkel excitons and charge-transfer excitons.[35]

■ ASSOCIATED CONTENT

Supporting Information

The Supporting Information is available free of charge at https://pubs.acs.org/doi/10.1021/acsomega.2c01987.

XRD data, more VIS data, and unsmoothed EELS dispersion data (PDF)

■ AUTHOR INFORMATION

Corresponding Author

Lukas Graf − *IFW Dresden, 01069 Dresden, Germany;* orcid.org/0000-0001-5799-4665; Email: l.graf@ifw-dresden.de

Authors

Fupin Liu − *IFW Dresden, 01069 Dresden, Germany;* orcid.org/0000-0002-8454-726X

Marco Naumann − *IFW Dresden, 01069 Dresden, Germany*

Friedrich Roth − *Institute of Experimental Physics, TU Bergakademeie Freiberg, 09599 Freiberg, Germany; Center for Efficient High Temperature Processes and Materials Conversion (ZeHS), TU Bergakademie Freiberg, 09599 Freiberg, Germany*

Bipasha Debnath − *IFW Dresden, 01069 Dresden, Germany*

Bernd Büchner − *IFW Dresden, 01069 Dresden, Germany*

Yulia Krupskaya − *IFW Dresden, 01069 Dresden, Germany*

Alexey A. Popov − *IFW Dresden, 01069 Dresden, Germany;* orcid.org/0000-0002-7596-0378

Martin Knupfer − *IFW Dresden, 01069 Dresden, Germany*

Complete contact information is available at: https://pubs.acs.org/10.1021/acsomega.2c01987

Notes

The authors declare no competing financial interest.

■ ACKNOWLEDGMENTS

Diffraction data were collected on BL14.2 at the BESSY II electron storage ring operated by the Helmholtz-Zentrum Berlin. We appreciate the help and support of Dr. Manfred Weiss and his team during the experiments at BESSY II. We are grateful to R. Hübel and F. Thunig for technical assistance. Financial support by the Deutsche Forschungsgemeinschaft within Project nos. KN393/25, KN393/26, KR4364/4, and PO1602/5 is gratefully acknowledged. The publication of this article was funded by the Open Access Fund of the Leibniz Association.

■ REFERENCES

(1) Kepler, R. G. Charge Carrier Production and Mobility in Anthracene Crystals. *Phys. Rev.* **1960**, *119*, 1226−1229.

(2) Aleshin, A. N.; Lee, J. Y.; Chu, S. W.; Kim, J. S.; Park, Y. W. Mobility studies of field-effect transistor structures basedon anthracene single crystals. *Appl. Phys. Lett.* **2004**, *84*, 5383−5385.
(3) de Boer, R. W. I.; Klapwijk, T. M.; Morpurgo, A. F. Field-effect transistors on tetracene single crystals. *Appl. Phys. Lett.* **2003**, *83*, 4345−4347.
(4) Jurchescu, O. D.; Baas, J.; Palstra, T. T. M. Effect of impurities on the mobility of single crystal pentacene. *Appl. Phys. Lett.* **2004**, *84*, 3061−3063.
(5) Kitamura, M.; Arakawa, Y. Pentacene-based organic field-effect transistors. *J. Phys.: Condens. Matter* **2008**, *20*, 184011.
(6) Chu, C.-W.; Shao, Y.; Shrotriya, V.; Yang, Y. Efficient photovoltaic energy conversion in tetracene-C60 based heterojunctions. *Appl. Phys. Lett.* **2005**, *86*, 243506.
(7) Kim, Y.-H.; Jeong, H.-C.; Kim, S.-H.; Yang, K.; Kwon, S.-K. High-Purity-Blue and High-Efficiency Electroluminescent Devices Based on Anthracene. *Adv. Funct. Mater.* **2005**, *15*, 1799−1805.
(8) Hepp, A.; Heil, H.; Weise, W.; Ahles, M.; Schmechel, R.; von Seggern, H. Light-Emitting Field-Effect Transistor Based on a Tetracene Thin Film. *Phys. Rev. Lett.* **2003**, *91*, 157406.
(9) Karl, N. Charge carrier transport in organic semiconductors. *Synth. Met.* **2003**, *133*, 649−657.
(10) Gershenson, M.; Podzorov, V.; Morpurgo, A. Colloquium: Electronic transport in single-crystal organic transistors. *RMP* **2006**, *78*, 973.
(11) Kera, S.; Yamane, H.; Ueno, N. First-principles measurements of charge mobility in organic semiconductors: Valence hole−vibration coupling in organic ultrathin films. *Prog. Surf. Sci.* **2009**, *84*, 135−154.
(12) Burdett, J. J.; Müller, A. M.; Gosztola, D.; Bardeen, C. J. Excited state dynamics in solid and monomeric tetracene: The roles of superradiance and exciton fission. *J. Chem. Phys.* **2010**, *133*, 144506.
(13) Troisi, A. Charge transport in high mobility molecular semiconductors: classical models and new theories. *Chem. Soc. Rev.* **2011**, *40*, 2347−2358.
(14) Burdett, J. J.; Bardeen, C. J. The dynamics of singlet fission in crystalline tetracene and covalent analogs. *Acc. Chem. Res.* **2013**, *46*, 1312−1320.
(15) Wilson, M. W.; Rao, A.; Ehrler, B.; Friend, R. H. Singlet exciton fission in polycrystalline pentacene: from photophysics toward devices. *Acc. Chem. Res.* **2013**, *46*, 1330−1338.
(16) Cudazzo, P.; Sottile, F.; Rubio, A.; Gatti, M. Exciton dispersion in molecular solids. *J. Phys.: Condens. Matter* **2015**, *27*, 113204.
(17) Hestand, N. J.; Spano, F. C. Expanded theory of H-and J-molecular aggregates: the effects of vibronic coupling and intermolecular charge transfer. *Chem. Rev.* **2018**, *118*, 7069−7163.
(18) Broch, K.; Dieterle, J.; Branchi, F.; Hestand, N. J.; Olivier, Y.; Tamura, H.; Cruz, C.; Nichols, V. M.; Hinderhofer, A.; Beljonne, D.; Spano, F. C.; Cerullo, G.; Bardeen, C. J.; Schreiber, F. Robust singlet fission in pentacene thin films with tuned charge transfer interactions. *Nat. Commun.* **2018**, *9*, 954.
(19) Davydov, A. S. the Theory of Molecular Excitons. *SOV PHYS USPEKHI* **1964**, *7*, 145−178.
(20) Schlosser, D. W.; Philpott, M. R. Singlet excitons in crystalline naphthalene, antracene, tetracene and pentacene. *Chem. Phys.* **1980**, *49*, 181−199.
(21) Bounds, P. J.; Siebrand, W. Charge-transfer excitons in anthracene crystals and their role in optical charge carrier generation. *Chem. Phys. Lett.* **1980**, *75*, 414−418.
(22) Sebastian, L.; Weiser, G.; Bässler, H. Charge transfer transitions in solid tetracene and pentacene studied by electroabsorption. *J. Chem. Phys.* **1981**, *61*, 125−135.
(23) Petelenz, B.; Petelenz, P.; Shurvell, H. F.; Smith, V. H. Reconsideration of the electroabsorption spectra of the tetracene and pentacene crystals. *Chem. Phys.* **1988**, *119*, 25−39.
(24) Slawik, M.; Petelenz, P. Theoretical interpretation of the electroabsorption spectra of polyacene crystals. II. Charge-transfer states. *J. Chem. Phys.* **1999**, *111*, 7576−7582.
(25) Petelenz, P.; Slawik, M.; Yokoi, K.; Zgierski, M. Z. Theoretical calculation of the electroabsorption spectra of polyacene crystals. *J. Chem. Phys.* **1996**, *105*, 4427−4440.
(26) Tiago, M. L.; Northrup, J. E.; Louie, S. G. Ab initio calculation of the electronic and optical properties of solid pentacene. *Phys. Rev. B* **2003**, *67*, 115212.
(27) Lim, S.-H.; Bjorklund, T. G.; Spano, F. C.; Bardeen, C. J. Exciton Delocalization and Superradiance in Tetracene Thin Films and Nanoaggregates. *Phys. Rev. Lett.* **2004**, *92*, 107402.
(28) Hummer, K.; Ambrosch-Draxl, C. Electronic properties of oligoacenes from first principles. *Phys. Rev. B* **2005**, *72*, 205205.
(29) Schuster, R.; Knupfer, M.; Berger, H. Exciton band structure of pentacene molecular solids: Breakdown of the Frenkel exciton model. *Phys. Rev. Lett.* **2007**, *98*, 037402.
(30) Gisslén, L.; Scholz, R. Crystallochromy of perylene pigments: Interference between Frenkel excitons and charge-transfer states. *Phys. Rev. B* **2009**, *80*, 115309.
(31) Gisslén, L.; Scholz, R. Crystallochromy of perylene pigments: Influence of an enlarged polyaromatic core region. *Phys. Rev. B* **2011**, *83*, 155311.
(32) Mazur, G.; Petelenz, P.; Slawik, M. Transition dipole moments of charge transfer excitations in one-component molecular crystals. *Chem. Phys.* **2012**, *397*, 92−97.
(33) Stradomska, A.; Kulig, W.; Slawik, M.; Petelenz, P. Excited-state polarizability in crystalline sexithiophene: Charge-transfer and vibronic effects. *Chem. Phys. Lett.* **2012**, *529*, 27−30.
(34) Yamagata, H.; Norton, J.; Hontz, E.; Olivier, Y.; Beljonne, D.; Brédas, J.-L.; Silbey, R.; Spano, F. The nature of singlet excitons in oligoacene molecular crystals. *J. Chem. Phys.* **2011**, *134*, 204703.
(35) Hestand, N. J.; Yamagata, H.; Xu, B.; Sun, D.; Zhong, Y.; Harutyunyan, A. R.; Chen, G.; Dai, H. L.; Rao, Y.; Spano, F. C. Polarized absorption in crystalline pentacene: Theory vs experiment. *J. Phys. Chem. C* **2015**, *119*, 22137−22147.
(36) Hestand, N. J.; Spano, F. C. Molecular Aggregate Photophysics beyond the Kasha Model: Novel Design Principles for Organic Materials. *Acc. Chem. Res.* **2017**, *50*, 341−350.
(37) Mahns, B.; Roth, F.; König, A.; Grobosch, M.; Knupfer, M.; Hahn, T. Electronic properties of 1,2;8,9-dibenzopentacene thin films: A joint experimental and theoretical study. *Phys. Rev. B* **2012**, *86*, 035209.
(38) Otto, F.; Huempfner, T.; Schaal, M.; Udhardt, C.; Vorbrink, L.; Schroeter, B.; Forker, R.; Fritz, T. Ordered Growth and Electronic Properties of 1,2:8,9-Dibenzopentacene (trans-DBPen) on Ag(111). *J. Phys. Chem. C* **2018**, *122*, 8348−8355.
(39) Tovstopyat, A.; Zojer, E.; Leising, G. Electronic Properties of 1,2;8,9-Dibenzopentacene in Solutions, Solid Matrices, and Thin Films. *J. Appl. Spectrosc.* **2016**, *83*, 20−26.
(40) Xue, M.; Cao, T.; Wang, D.; Wu, Y.; Yang, H.; Dong, X.; He, J.; Li, F.; Chen, G. F. Superconductivity above 30 K in alkali-metal-doped hydrocarbon. *Sci. Rep.* **2012**, *2*, 389.
(41) Zhong, G.-H.; Zhang, C.; Yan, X.; Li, X.; Du, Z.; Jing, G.; Ma, C. Structural and electronic properties of potassium-doped 1,2;8,9-dibenzopentacene superconductor: comparing with doped [7]-phenacenes. *Mol. Phys.* **2017**, *115*, 472−483.
(42) Roth, F.; König, A.; Mahns, B.; Büchner, B.; Knupfer, M. Evidence for phase formation in potassium intercalated 1,2;8,9-dibenzopentacene. *Eur. Phys. J. B* **2012**, *85*, 242.
(43) Laudise, R. A.; Kloc, C.; Simpkins, P. G.; Siegrist, T. Physical vapor growth of organic semiconductors. *J. Cryst. Growth* **1998**, *187*, 449−454.
(44) Mueller, U.; Förster, R.; Hellmig, M.; Huschmann, F. U.; Kastner, A.; Malecki, P.; Pühringer, S.; Röwer, M.; Sparta, K.; Steffien, M.; Ühlein, M.; Wilk, P.; Weiss, M. S. The macromolecular crystallography beamlines at BESSY II of the Helmholtz-Zentrum Berlin: Current status and perspectives. *Eur. Phys. J. Plus* **2015**, *130*, 141.
(45) Sparta, K. M.; Krug, M.; Heinemann, U.; Mueller, U.; Weiss, M. S. Xdsapp2.0. *J. Appl. Crystallogr.* **2016**, *49*, 1085−1092.
(46) Kabsch, W. XDS. *Acta Crystallogr. D* **2010**, *66*, 125−132.

https://doi.org/10.1021/acsomega.2c01987
ACS Omega 2022, 7, 21183−21191

(47) Sheldrick, G. M. Crystal structure refinement with SHELXL. *Acta Crystallogr. C* **2015**, *71*, 3−8.
(48) Fink, J. In *Recent Developments in Energy-Loss Spectroscopy*; Hawkes, P. W., Ed.; Advances in Electronics and Electron Physics; Academic Press: 1989; Vol. 75, pp 121−232.
(49) Roth, F.; König, A.; Fink, J.; Büchner, B.; Knupfer, M. Electron Energy-Loss Spectroscopy: A versatile tool for the investigations of plasmonic excitations. *J. Electron Spectrosc.* **2014**, *195*, 85−95.
(50) Holmes, D.; Kumaraswamy, S.; Matzger, A. J.; Vollhardt, K. P. C. On the Nature of Nonplanarity in the [N]Phenylenes. *Chem. Eur. J.* **1999**, *5*, 3399−3412.
(51) Perkampus, H. H.; Pohl, L. Zur Davidov-Aufspaltung in den Absorptionsspektren dünner Filme einiger aromatischer Kohlenwasscrstoffe. *Theor. Chem. Acc.* **1963**, *1*, 116−123.
(52) Köhler, A.; Bässler, H. *Electronic Processes in Organic Semiconductors: An Introduction*; Wiley: 2015; pp 1−405.
(53) Fox, M. *Optical properties of solids*; Oxford University Press: 2002.
(54) Puschnig, P.; Ambrosch-Draxl, C. Atomistic modeling of optical properties of thin films. *Adv. Eng. Mater.* **2006**, *8*, 1151−1155.
(55) Puschnig, P.; Ambrosch-Draxl, C. First-principles approach to the understanding of π-conjugated organic semiconductors. *Monatsh. Chem.* **2008**, *139*, 389−399.
(56) Faltermeier, D.; Gompf, B.; Dressel, M.; Tripathi, A. K.; Pflaum, J. Optical properties of pentacene thin films and single crystals. *Phys. Rev. B* **2006**, *74*, 125416.
(57) Bree, A.; Lyons, L. 1002. The intensity of ultraviolet-light absorption by monocrystals. Part IV. Absorption by naphthacene of plane-polarized light. *J. Chem. Soc.* **1960**, 5206−5212.
(58) Knupfer, M.; Fink, J.; Armbruster, J. F.; Romberg, H. A. Preparation and electronic structure of phase pure K3C60. *Z. Phys. B* **1995**, *98*, 9−15.
(59) Grobosch, M.; Schuster, R.; Pichler, T.; Knupfer, M.; Berger, H. Analysis of the anisotropy of excitons in pentacene single crystals using reflectivity measurements and electron energy-loss spectroscopy. *Phys. Rev. B* **2006**, *74*, 155202.
(60) Flatz, K.; Grobosch, M.; Knupfer, M. The electronic excitation spectrum of CuPcF16 films. *Appl. Phys. A: Mater. Sci. Process.* **2009**, *94*, 179−183.
(61) Roth, F.; Nohr, M.; Hampel, S.; Knupfer, M. Low-energy exciton pocket at finite momentum in tetracene molecular solids. *EPL* **2015**, *112*, 37004.
(62) Roth, F.; Cudazzo, P.; Mahns, B.; Gatti, M.; Bauer, J.; Hampel, S.; Nohr, M.; Berger, H.; Knupfer, M.; Rubio, A. Loss spectroscopy of molecular solids: combining experiment and theory. *New J. Phys.* **2013**, *15*, 125024.
(63) Roth, F.; Schuster, R.; König, A.; Knupfer, M.; Berger, H. Momentum dependence of the excitons in pentacene. *J. Chem. Phys.* **2012**, *136*, 204708.
(64) Dressel, M.; Grüner, G. *Electrodynamics of solids: optical properties of electrons in matter*; Cambridge University Press: 2002.

https://doi.org/10.1021/acsomega.2c01987
ACS Omega 2022, 7, 21183−21191